Fiber Link Design Considerations for Cloud-Radio Access Networks

(Invited Paper)

Nathan J. Gomes, *Senior Member, IEEE*, Philippos Assimakopoulos, Luis C. Vieira*, and Pavlos Sklikas
Broadband and Wireless Communications Group, University of Kent, Canterbury, United Kingdom
*DAELN, Universidade Tecnológica Federal do Paraná, Curitiba, Brazil
N.J.Gomes@kent.ac.uk

***Abstract*—Analog radio over fiber (RoF) links may offer advantages for cloud-Radio Access Networks in terms of component cost, but the behavior of the distortion with large numbers of subcarriers needs to be understood. In this paper, this is presented in terms of the variation between subcarriers. Memory polynomial predistortion is also shown to compensate for RoF and wireless path distortion. Whether for digitized or analog links, it is shown that appropriate framing structure parameters must be used to assure performance, especially of time-division duplex systems.**

Keywords—Cloud-RAN, Long-term evolution-advanced, OFDM, OFDMA, digital predistortion, Medium Access Control.

I. INTRODUCTION

Cloud-Radio Access Networks (C-RANs) have been proposed for new mobile communication systems in order to provide for high-throughput high user population densities [1], [2]. The shortened wireless transmission distance between user and distributed antenna (or remote radio head) provides increased data-rates and lower transmit powers, while centralization of the baseband functions has been shown to improve energy efficiency [1], as well as offering the possibilities for performance enhancement through centralized resource management, interference cancellation schemes and coordinated multipoint transmission [2]. With centralized base station pools covering larger areas through numerous remote radio heads, backhaul requirements may be lessened. However, stringent requirements are now placed on the "fronthaul", where the fiber distribution system has become part of the radio access network. Such requirements relate not only to the bandwidth for carrying the multiple duplex radio transmissions to/from the remote radio heads, but also to latency and jitter, especially if cooperative transmission/reception schemes are to be used [2]. These may require signals to be received/transmitted through different fiber lengths within fractions of a symbol period.

Currently, digitized fibre links, following industry standards such as the Common Public Radio Interface (CPRI) or Open Base station Architecture Initiative (OBSAI) are envisaged for the interconnections between base station baseband units and remote radio heads [1], [3]. However, bit-rate requirements for wide-bandwidth future mobile systems increase rapidly, especially when multiple signals are transported to/from each remote radio head; for example, using the same oversampling and sample lengths proposed for 20 MHz, signals, it is predicted that 24 Gbps data rate links are required for the transport of 4 100 MHz radio channels [4]. For this reason, the use of analog radio over fiber (RoF) has been proposed in [4]. While analog RoF reduces the bandwidth and therefore cost of the fiber optic links, concerns remain about achieving the necessary performance, especially as next generation mobile systems may aggregate spectrum with large total numbers of OFDM subcarriers, and therefore large potential peak-to-average-power ratios (PAPRs). Linearization techniques have been proposed to counteract the distortion experienced by such signals [5] Whether analog or digitized radio links are used, a further problem arises with increased latency in the access network because of the long fiber delays (compared to typical wireless propagation delays). Such delays mean that careful consideration must be given to the synchronization between the transmissions to/from different radio heads, and to the framing structures employed – timing advance mechanisms need to take into account fiber and wireless delays separately [6].

In this paper, we report on and extend previous work in three areas relevant to the design of fiber links for C-RANs. First, in Section II, assuming analog transmission, we report on the effect of PAPR increase with increasing numbers of subcarriers, as may occur when radio spectrum is aggregated. In particular, in this paper, we examine the non-uniform behavior that occurs across subcarriers with large IFFT sizes. Then, in Section III, and continuing the assumption of the use of analog RoF, we present possibilities for nonlinear distortion compensation at baseband using memory polynomial-based predistorters. In this work, we particularly examine performance of such predistorters over links consisting of both fiber and wireless paths. Finally, in Section IV, in work relevant to both analog and digitized RoF links, we investigate the effects of fiber delay in 3rd Generation Partnership Project (3GPP) Long-Term Evolution (LTE) Time-division Duplex (TD) transmission, particularly related to framing and synchronization. Here, for the first time, the work is extended to examine the effect on the random access channel procedure for gaining initial access and timing synchronization.

II. PAPR ISSUES IN LTE-A AND EVM

An OFDM signal consists of a large number of modulated subcarriers, which dependent on their phases, can result in

The work reported was supported in part by the European Union under grant agreement FP7-ICT-2007-215533 FUTON.

high instantaneous amplitudes, much higher than the signal's average amplitude. As a result, the composite envelope may infringe upon more nonlinear parts of the channel's power transfer function leading to distortion. This is particularly a problem for LTE-Advanced where the number of subcarriers is potentially very large because of spectrum aggregation. Variations around the average amplitude of the composite envelope for the baseband OFDM signal *x[n]*, can be quantified through the PAPR factor [7], given as

$$PAPR(x[n])_{0-(N-1)} = \frac{\max\left\{|x[n]|^2\right\}}{\mathrm{E}\left\{|x[n]|^2\right\}}, \quad (1)$$

where N is the number of data subcarriers in a single OFDM symbol and E{.} is the expectation operator.

The formulation in (1) simply gives the average PAPR for a single OFDM symbol. A more useful PAPR measure is one that takes into account a number of transmitted OFDM symbols, leading to a statistical PAPR formulation. Then, the Probability Density Function (PDF) of the statistical PAPR for an up-converted OFDM signal *x(t)*, that is one that is modulating an RF carrier, is given as [8]

$$p_{PAPR}(g) = \frac{d}{dg}\left\{\frac{1}{2}\left[1+\mathrm{erf}\left(\sqrt{\frac{g}{2}}\right)\right]^{lN}\right\}, \quad (2)$$

where erf is the error function, $g = x^2(t)/\sigma^2$ with σ^2 being the variance of the In-phase and Quadrature components of the OFDM signal, and l is an empirical fitting factor.

The result of (2) for different IFFT sizes is shown in Fig. 1, where the median points of the individual distributions are also noted. From this result, it would be expected that the larger the number of data subcarriers in a signal, the more prone to distortion that signal will be, meaning that it will require greater input power back-off to reduce distortion effects. However, a typical EVM measurement given as

$$EVM(\%rms) = 100\frac{1}{S}\sum_{s=1}^{S}\sqrt{\frac{\frac{1}{N}\sum_{n=0}^{N-1}\left[\left(I\{X_r - X_i\}\right)^2 + \left(Q\{X_r - X_i\}\right)^2\right]}{\frac{1}{N}\sum_{n=0}^{N-1}\left[\left(I\{X_i\}\right)^2 + \left(Q\{X_i\}\right)^2\right]}}, \quad (3)$$

with X_r the received symbol, X_i the ideal symbol from a given QAM constellation point and S the number of OFDM symbols, does not indicate any difference in performance between different IFFT sizes (at least to a level expected by the PAPR results) as shown in Fig. 2.

To this extent, in [8] it was shown that the median (and not the mean) of the EVM is directly related to the median of the statistical PAPR. This is due to the effects of distortion, which, unlike those of white noise, lead to varying skew EVM distributions with the skew being higher for lower IFFT sizes. In [9] it was further shown that in the limiting case of an abrupt nonlinearity (soft-limiter), the relation between the median values of the statistical PAPR and EVM is exact. Furthermore, the skew in the EVM distributions has an effect on the Symbol-Error Rate (SER) as follows [9]: For small modulation levels (e.g. QPSK), larger IFFT sizes will tend to produce errors at lower input powers (compared to smaller IFFT sizes). However, for large modulation levels (e.g. 64-QAM) the opposite is true: Smaller IFFT sizes produce errors at lower input powers (compared to larger IFFT sizes). Therefore, there is an opposing effect: Smaller IFFT sizes, will generally have smaller effective PAPR and better EVM performance, but may have worse SER performance (under higher modulation levels).

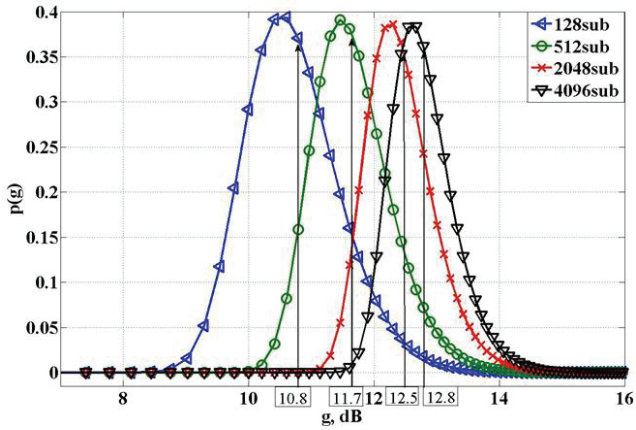

Fig.1. Probability distribution function for the effective (statistical) PAPR for different IFFT sizes.

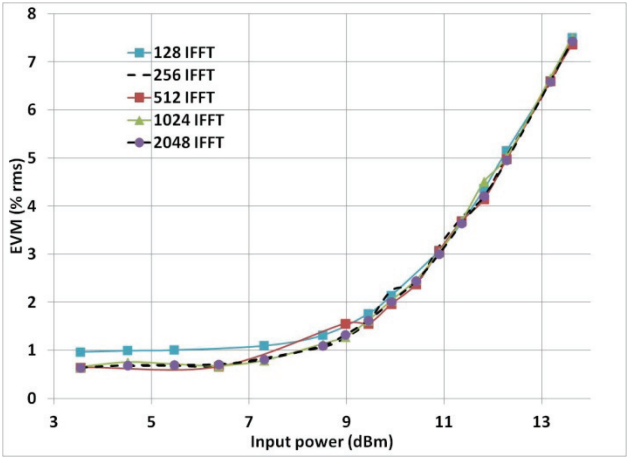

Fig.2. Measured mean EVM results with varying RF input power for different IFFT sizes.

For OFDMA systems such as LTE it is important to note how distortion affects subcarriers at different locations in the signal band. Fig. 3 shows EVM performance results with varying RF input power for subcarriers located in different positions in the signal band for 4096 and 512 IFFT sizes, over 450 transmitted OFDM symbols in total. Specifically, the EVM performance at the edge of the band, is measured over

the 152nd subcarrier from the edge of the band for the 4096 IFFT signal and the 19th subcarrier for the 512 IFFT signal. The EVM performance at the middle of the band is measured over subcarriers that are located at the same relative distances from the middle of the band. Note that the chosen subcarriers (at the edge or the middle of the band) for the two signals occupy the same position (approximately) within the signal band. At lower input powers, the EVM for the subcarrier at the edge of the band is higher for this specific optical link and this is due to I and Q offset effects that predominately affect the edge subcarriers. As the power is increased, the mean EVM for the subcarrier at the middle of the band increases at a faster rate and eventually surpasses the EVM at the edge of the band. This is a clear indication that once distortion dominates, it does not behave as white noise and instead behaves more like colored noise affecting the subcarriers in the middle of the band to a larger extent. This behavior is more clearly evident in the 4096 IFFT signal.

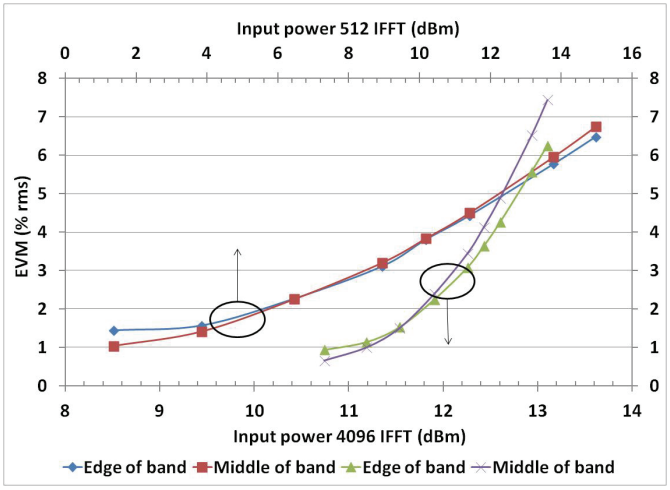

Fig. 3. EVM measured results for subcarriers located in the middle and the edge of the signal band for 512 and 4096 IFFT sizes.

The two EVM traces meet at an input power of approximately 10.6 dBm for the 512 IFFT signal and 9.6 dBm for the 4096 IFFT signal. This difference in power is close in value to the difference in the median of the statistical PAPR between the two signals (~1.1 dB) shown in Fig.1.

III. Digital Predistortion of RoF Links

Digital predistortion has been proposed and demonstrated for the compensation of RoF link nonlinearity at baseband [5], [10] – [12]. With this approach, adaptive signal processing techniques are used to model the inverse function of the RoF nonlinearity, i.e. to obtain a predistorter model. The predistorter is then inserted in cascade with the RoF link so as to linearize the system.

In early works, simulation results on the performance of digital predistortion for directly modulated RoF links were reported [10]. The RoF link was represented by a third-order polynomial model, obtained from measurements on a 2.2-km 1.8-GHz DFB RoF link and using a single-carrier quadrature phase shift keying (QPSK) input signal. In [12], a digital predistortion approach to directly modulated RoF links was proposed, based on memory polynomials. This approach was experimentally demonstrated in [5], at an intermediate frequency (IF) of 50 MHz. Performance comparisons of adaptive algorithms for predistortion identification were made, with the predistorter trained either using a least mean squares (LMS), a recursive least squares (RLS), or a LMS/RLS identification algorithm. In that work, the predistorter was implemented in hardware, with both the RoF memory effects and static nonlinearity reduced. The memory-polynomial-based digital predistortion approach was later on tested significantly closer to (and around) the laser resonance frequency (from 2.47 to 3.7 GHz), with the resilience of the approach to changes in average power levels and in modulation level of QAM schemes also investigated [13].

Here, an experiment on digital predistortion for the RoF link cascaded with the wireless path is reported. This would enable predistorter training at the mobile terminal and its coefficients sent back to the CU for updating the predistorter. In Fig. 4, the setup used for this experiment is depicted. An OFDM signal with 256 subcarriers, 18-MHz bandwidth, and four times oversampling is used. The data modulation is 64QAM. The RoF link here consists of 20-km standard single-mode fiber a 1311-nm DFB laser and PIN photodiode. The results are obtained at a carrier frequency of 2.47 GHz. The predistorter is trained with the laser driven at 0-dBm average power. A 17-dB amplifier with 1-dB compression point of 26 dBm (output) is used before the laser. An amplifier with gain of 21.3 dB, model Mini-Circuits ZX60-2522M-S+, is inserted between the RoF link output and the transmitter antenna. At the receiver end, two amplifiers are used before the spectrum analyzer, with total gain of 34.8 dB. The wireless range is 2 m. The measured signals are captured after the wireless path by the VSA 89600 and processed in Matlab.

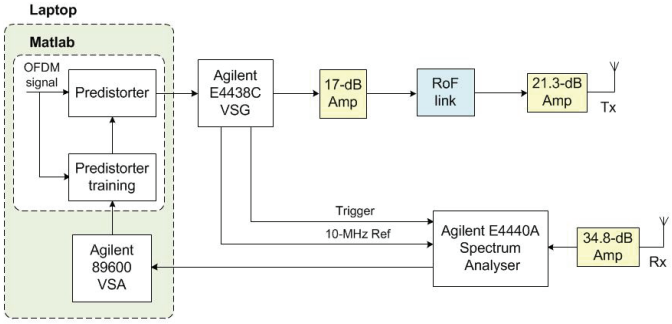

Fig. 4 Setup for predistortion compensation of RoF and wireless links

The receiver antenna, preamplifiers, and VSA/spectrum analyser in the experimental setup simulate the mobile terminal, considering the downlink direction of a RoF-wireless link. The predistorter is implemented in Matlab before the VSG, as shown in Fig. 4. The VSG performs I/Q to IF and digital-to-analog (D/A) conversions, and IF to RF up-conversion, similar to what is done by a real digital transmitter at the CU. The RF amplifier and DFB laser of the experimental setup would also be located at the CU. It should be noted that, in this work, the predistorter is trained off-line in Matlab. Considering the downlink transmission of a real

RoF-wireless system, the training algorithm can be implemented either at the mobile terminal or at the CU. However, the predistorter itself has to be implemented at the CU.

The predistorter output z is given by:

$$z(n) = \sum_{k=1}^{K} \sum_{q=0}^{Q} c_{kq} x(n-q) \left| x(n-q) \right|^{k-1} \quad (4)$$

where x is the input signal, c_{kq} are the polynomial coefficients, and K and Q are the predistorter nonlinearity order and memory length, respectively. For this experiment, K is set to 7 and Q to either 0 (memorless predistorter) or 2 (memory predistorter).

EVM values of 8.46 % for the non-predistorted link, 8.13 % for the compensated link with memoryless predistortion, and 2.52 % for the compensated link with memory predistortion were obtained. The significant difference found for the EVMs for the memoryless against the memory predistortion approaches indicates that memory predistortion is necessary when the wireless path is included in the link to be compensated (note that no equalization technique is implemented at the mobile terminal). The average received power at the VSA was more unstable during the measurements (due to the wireless multipath) compared to the measured power after the photodiode. In spite of that, the EVM of 2.52 % obtained here using memory predistortion is close to the EVM of 2.1 % found when the same predistortion approach is applied to only the RoF link.

From the PSDs plotted in Fig.5, we can see that both memoryless and memory predistorters can reduce spectral regrowth. The lower/upper adjacent channel power ratios (ACPRs) of the non-predistorted link are -30.5 and -33.3 dBc, respectively. For the memoryless predistortion case, lower/upper ACPRs of -42.0/-43.1 dBc are achieved, while lower/upper ACPRs of -40.4/-43.7 dBc are achieved using the memory predistortion approach.

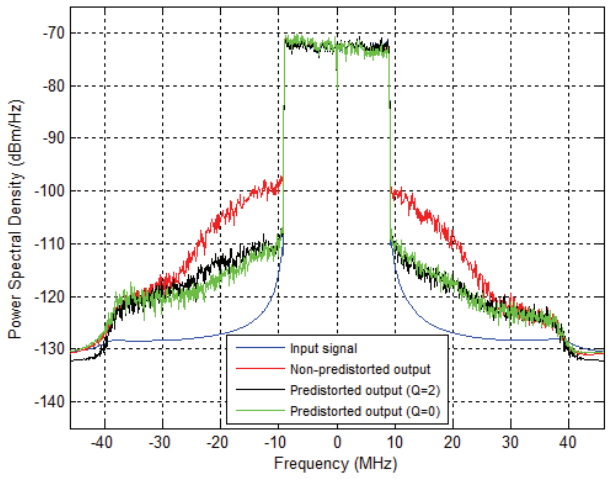

Fig. 5. Spectral regrowth due to distortion for non-predistorted and predistorted RoF links.

This experiment can be seen as a proof of concept. In order to obtain a deeper understanding of the predistortion technique for systems with RoF transmission plus wireless path, further work needs to be carried out using larger wireless ranges.

IV. Fiber Delay Effects

The insertion of fiber links in C-RAN systems leads to increased propagation delay which may affect the performance of the physical (PHY) and Medium Access Control (MAC) layer protocols and procedures of the wireless technologies under consideration. In this section we present the optical distribution network's impact on the TD-LTE random access (RACH) procedure and the Evolved NodeB to User Equipment (eNB-UE) downlink-uplink (DL-UL) timing synchronization, as well as the mitigation of the optical multipath and Inter Symbol Interference (ISI) caused by it.

A. Random Access Procedure for Timing Synchronization

One of the main functions of the RACH procedure in LTE is its use by UEs during initial access for the acquisition of UL timing . Although UEs synchronize to the received DL signal before any RACH transmission in the Physical Random Access Channel (PRACH), there is a timing uncertainty in the RACH transmissions caused by the round-trip delay (RTD); the start of an UL subframe at the UE is defined relative to the start of a DL subframe received at the UE [14]-[16]. The PRACH duration limits the maximum optical fiber length (L_{max_RACH}) supported by the RACH procedure in C-RAN systems. Thus, the additional optical propagation delay has to be taken into account in order for the UEs' RACH transmissions to be received at the eNB within the PRACH enabling the UEs' RTD to be correctly measured.

TABLE I. TD-LTE RACH Preamble Parameters.

	RACH Preamble Format				
	0	**1**	**2**	**3**	**4**
Subframes occupied	1 (1 ms)	2 (2 ms)	2 (2 ms)	3 (3 ms)	UpPTS
CP duration T_{CP}(µs)	103.13	684.38	203.13	684.38	14.58
Preamble Sequence duration T_{SEQ}(µs)	800	800	2×800 = 1600	2×800 = 1600	133.33
Guard Period duration (µs)	96.88	515.63	196.88	715.63	9.37
Max. delay spread(µs)	6.25	16.67	6.25	16.67	5.21
Max. fiber length L_{max_RACH}(km)	10.022	53.341	20.366	69.073	0.969

TD-LTE systems support five different RACH preamble formats [14] for the network entry RACH procedure. The typical RACH preamble format is Format 0, with Formats 1 to 3 used when larger cells need to be supported. Then, there is preamble Format 4, applicable to very small cells only due to its short duration, known as the short RACH (S-RACH) [14]. In general, greater cell sizes/greater timing uncertainties require a longer RACH preamble Cyclic Prefix (CP) and RACH guard period [16]. The RACH preamble CP has to be longer than the sum of the RTD of the supported cell size plus

the maximum delay spread of the channel, whereas the guard period has to be sufficient for the accommodation of the RTD of the supported cell size [16]. Table I contains the different RACH preamble format supported in TD-LTE systems with the maximum fiber length for C-RAN systems allowed by each [16], [17].

B. TD-LTE DL-UL Timing Synchronization

For TD-LTE a total of seven DL/UL frame configurations are defined in [18]; each subframe in the frame is reserved as standard DL, standard UL or Special subframe. The Special subframe contains three fields: the DL Pilot Time Slot (DwPTS), the Guard Period (GP) and the UL Pilot Time Slot (UpPTS). The GP, which is created by adjusting the DwPTS [14], provides the transceivers adequate time to switch from transmit to receive state, and vice versa [18], thus allowing for eNB-UE DL-UL timing synchronization. The durations of DwPTS and UpPTS, and, as a result, the GP length, are configured by the network based on the cell's maximum RTD (i.e. the maximum cell size); various Special subframe configurations are defined in [18], as presented in [19]. However, the total length of DwPTS, GP and UpPTS is limited to 1ms [18]. In the case of TD-LTE C-RANs, the GP interval could accommodate the extra propagation delay due to the fiber links, and thus maintain the eNB-UEs DL-UL synchronization.

The duration of the GP interval (T_{GP}) is given by equation (5) [16]:

$$T_{GP} = RTD_{\max} + T_{UE}^{RxTx} + \max(T_{UE}^{TxRx}, T_{eNB}^{RxTx}) \quad (5)$$

where, $RTD_{\max}$ is the supported cell's maximum RTD, T_{UE}^{RxTx} and T_{eNB}^{RxTx} is the time the UE and the eNB, respectively, needs to switch from receive (Rx) to transmit (Tx) mode, T_{UE}^{TxRx} is the time the UE needs to switch from Tx to Rx mode and max($x1$, $x2$) returns the maximum number between $x1$ and $x2$. For our calculations we assume that each of the T_{UE}^{RxTx}, T_{eNB}^{RxTx} and T_{UE}^{TxRx} is equal to 20μs [14], [15]. Thus, with c representing the speed of light and n_f the refractive index of the optical fiber, the maximum optical fiber length ($L_{\max\_TDD}$) that can be accommodated by the GP, is given by equation (6):

$$L_{\max\_TDD} = \frac{\left[T_{GP} - T_{UE}^{RxTx} - \max(T_{UE}^{TxRx}, T_{eNB}^{RxTx})\right] \times c}{2 \times n_f} \quad (6)$$

Table II presents L_{max_TDD} for different special subframe configurations and CP durations. A negligible wireless propagation delay is assumed.

Based on the calculation of the TD-LTE DL PHY Data Rate (PDR_{DL}) for different special subframe configurations given in [19], Fig. 6 (a)-(b) depict the theoretical normalized PDR_{DL} (given the maximum PDR_{DL} is achieved when Special subframe configuration 4 and 3 is used for Normal and Extended CP in the DL, respectively) of a TD-LTE C-RAN system for Normal and Extended CP in the DL, respectively, when different Special subframe configurations are used. A 6:3 DL:UL subframe ratio [18] is assumed for the calculations. It is obvious that Special subframe configurations 0 and 5 (Fig. 6(a)), as well as Special subframe configurations 0 and 4 (Fig. 6(b)), allow longer optical links to be used in the distribution network, as the GP has longer duration for these configurations. However, if Special subframe configurations 0 and 5 or 0 and 4 are used when the Normal or Extended CP is used in the DL, a system performance degradation of 9.4% and 8.5% is caused, respectively. Moreover, longer optical fibers than 69.7 km or 66 km, for Normal or Extended CP in the DL, respectively, in TD-LTE C-RANs would cause the eNB-UEs DL-UL timing synchronization to be lost. Furthermore, the CP duration used in the UL does not seem to greatly affect the GP duration, and thus, the maximum allowed fiber length.

TABLE II. LMAX_TDD FOR SPECIAL SUBFRAME CONFIGURATIONS

Special Subframe Configuration	Normal CP in DL		Extended CP in DL	
	L_{max_TDD} (km)		L_{max_TDD} (km)	
	Normal CP in UL	*Extended CP in UL*	*Normal CP in UL*	*Extended CP in UL*
0	69.7	68.4	66	64.8
1	25.3	24.1	22.9	21.7
2	18	16.7	14.3	13.1
3	10.6	9.3	5.72	4.4
4	3.2	2	58.6	56.2
5	62.3	59.8	15.5	13.1
6	18	15.5	6.9	4.4
7	10.6	8.1	-	-
8	3.2	0.76	-	-

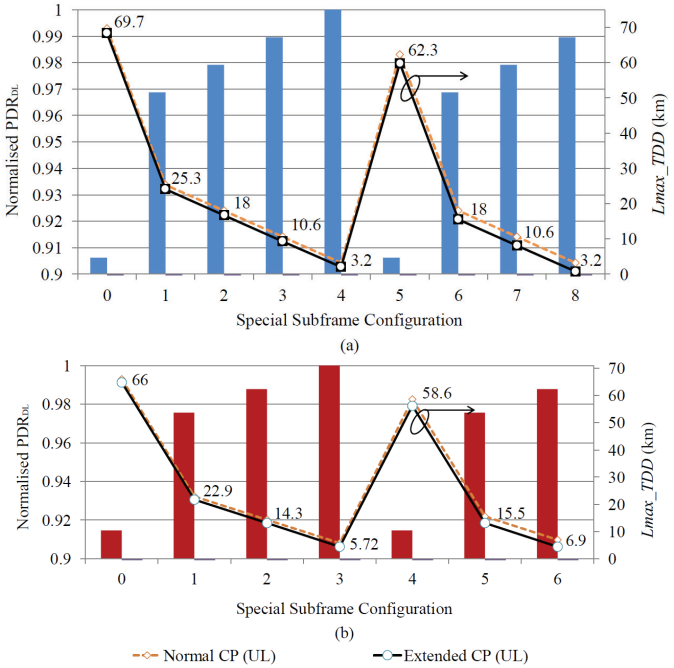

Fig. 6 TD-LTE Normalised PDR_{DL} vs. L_{max_TDD} for (a) Normal CP in DL, and (b) Extended CP in DL.

C. Mitigation of Optical Multipath Effect and ISI

In LTE C-RANs the CP, apart from preventing ISI due to the wireless propagation multipath, could also be exploited to eliminate the ISI caused by the optical distribution network due to its differences in optical fiber lengths. No ISI and performance degradation will occur due to the optical distribution network as long as the CP duration is longer than the delay difference between the different optical paths. It has been shown in [19] that the maximum difference in fiber lengths between the various LTE C-RAN RAUs supported by the Normal CP configuration can be up to 324m, whereas the Extended CP allows differences in fiber lengths of up to 1.15 km (assuming a negligible wireless delay spread).

Table III shows the effect of increasing the CP duration from Normal to Extended on system performance; it gives the PDR_{DL} performance degradation assuming 10 ms TD-LTE frames [18], for 3:1 DL-UL subframe ratio, and various Special subframe configurations. Table III shows that the PDR_{DL} performance degradation when the Extended CP is used instead of the Normal is almost the same for Special subframe configuration 0, 1, 2 and 3. In this case, as the CP duration is increased, the number of available DL data symbols per 10 ms TD-LTE frame (for each of the aforementioned Special subframe configurations) is reduced by 12-14 symbols. The most noticeable performance degradation of a TD-LTE system when the CP duration is increased from Normal to Extended is for Special subframe configuration 4 (maximum performance degradation) and 5 (minimum performance degradation); the DL data symbols are decreased by 30, and by 2, respectively.

TABLE III. SYSTEM PERFORMANCE DEGRADATION WHEN EXTENDED CP IS USED INSTEAD OF NORMAL CP.

Special Subframe Configuration	PDR_{DL} Decrease %
0	13.33
1	13.73
2	13.46
3	13.21
4	27.78
5	2.22
6	11.76
7	N/A
8	N/A

V. CONCLUSION

C-RANs offer throughput (e.g. in terms of enabling joint transmission and interference cancellation schemes) and energy efficiency advantages to forthcoming mobile communication systems. However, the bit-rate requirements for digitized radio links, especially if multiple signal transmission is required for MIMO/coordinated multipoint schemes, become very high. Analog radio over fiber can alleviate these requirements, but care needs to be taken with distortion effects on the OFDM radio signals. Predistortion with memory polynomials has been shown to compensate both fiber and radio links. While the TD-LTE standards provide mechanisms which make feasible the application of C-RANs, in order to preserve correct protocol operation and achieve the best performance for the desired optical network architecture, an accurate combination of adapted guard times, random access channel structure and CP is necessary.

REFERENCES

[1] *C-RAN: The Road Towards Green RAN*, China Mobile Res. Inst., White Paper, ed.2.5, Beijing, China, 2011

[2] N.J.Gomes, P. Monteiro, A. Gameiro (eds.), *Next Generation Wireless Communications Using Radio over Fiber*, Chichester, United Kingdom: Wiley, 2012

[3] B. Guo, W. Cao, A. Tao and D. Samardzija, "LTE/LTE-A signal compression on the CPRI interface", Bell Labs Technical J., vol.18, pp. 117-133, Sept. 2013

[4] D. Wake, A. Nkansah, and N.J. Gomes, "Radio over fiber link design for next generation wireless systems", *J. Lightw. Technol*., vol. 28, pp. 2456-2464, Aug. 2010

[5] A. Hekkala, M. Hiivala, M. Lasanen, J. Perttu, L. C. Vieira, N. J. Gomes, and A. Nkansah, "Predistortion of Radio Over Fiber Links: Algorithms, Implementation, and Measurements," *IEEE Trans, Circuits and Systems I: Regular Papers*, vol.59, no.3, pp.664-672, March 2012

[6] A. Hekkala et al., "Architectures for the joint compensation of nonideal RoF links", *IEEE Wireless Comm. Magazine*, vol.17, issue 3, pp. 52-59, June 2010

[7] J. Tellado, *Multicarrier modulation with low PAR-Applications to DSL and wireless*, Kluwer academic publishers, 2002.

[8] P. Assimakopoulos, A. Nkansah, N. J. Gomes and D. Wake, "Statistical distribution of EVM measurements for direct-modulation radio over fiber links transporting OFDM signals," *IEEE Trans. Microw. Theory Tech*., vol. 61, no. 4, pp. 1709–1717, Apr. 2013.

[9] P. Assimakopoulos, R. Santamaria, N.J. Gomes, "EVM and SER performance of OFDM signals with different IFFT sizes under nonlinear distortion," in *IEEE Intl. Conf. Communications (ICC), Workshop on Optical-Wireless Integrated Technologies for Systems and Networks*, pp. 848-852, Budapest, Hungary, June 2013.

[10] X. N. Fernando and A. B. Sesay, "Adaptive asymmetric linearization of radio over fiber links for wireless access," *IEEE Trans. Vehicular Technol.* vol. 51, pp. 1576-1586, Nov. 2002.

[11] H. Moon and R. Sedaghat, "FPGA-Based adaptive digital predistortion for radio-over-fiber links," *Microprocessors and Microsystems,* vol. 30, pp. 145-154, May 2006

[12] A. Hekkala, M. Lasanen, L. C. Vieira, N. J. Gomes, and A. Nkansah, "Architectures for Joint Compensation of RoF and PA with Nonideal Feedback", in *Proc. 2010 IEEE 71st Vehicular Technology Conference, VTC-Spring 2010*, Taipei, Taiwan, May 2010

[13] L.C. Vieira and N.J. Gomes, "Resilience of digital predistortion for OFDM-radio over fiber links near laser resonance", submitted to *IEEE Trans. Microw. Theory Tech.*, 2013

[14] H. Holma, A.Toskala, *LTE for UMTS, Evolution to LTE-Advanced*, Second ed. Chichester, United Kingdom: Wiley, 2011.

[15] E.Dahlman, S. Parkvall, J. Sköld, *4G LTE/LTE-Advanced for Mobile Broadband,* Oxford, UK: Academic Press, 2011.

[16] Sesia, I. Toufik, M. Baker, *LTE – The UMTS Long Term Evolution From Theory to Practice*, Second ed. Chichester, United Kingdom: Wiley, 2011.

[17] F. Khan, *LTE for 4G Mobile Broadband Air Interface Technologies and Performance,* New York, USA: Cambridge University Press, 2009.

[18] *LTE; Evolved Universal Terrestrial Radio Access (E-UTRA); Physical channels and modulation (3GPP TS 36.211 version 10.4.0 Release 10)*, in ETSI TS 36 V 0.4.0, ed, 2012.

[19] P. Sklikas, N. J. Gomes, "Downlink-uplink timing synchronization and optical multipath limitations in 3GPP TD-LTE Radio-over-Fiber networks," *Int. Topical Meeting Microwave Photonics (MWP2012),* pp.212-215, Sept. 2012.